Novel ROS-Responsive Marine Biomaterial Fucoidan Nanocarriers with AIE Effect and Chemodynamic Therapy

Chunjing Guo
Ocean University of China
Qiang Chen
Yantai University
Xue Liu
Yantai University
Ziting Cheng
Yantai University
Daquan Chen (cdq1981@126.com)
Yantai University https://orcid.org/0000-0002-6796-0204
Ming Kong
Ocean University of China

Short Communication

Keywords: Chemodynamic therapy, Reactive oxygen species, Aggregation-induced emission, Fucoidan, Paclitaxel

Posted Date: September 23rd, 2021

DOI: https://doi.org/10.21203/rs.3.rs-882577/v1

Version of Record: A version of this preprint was published at International Journal of Biological Macromolecules on January 1st, 2022. See the published version at https://doi.org/10.1016/j.ijbiomac.2022.01.060.

Abstract

Chemodynamic therapy (CDT) has been widely used in the treatment of many kinds of tumors, which can effectively induce tumor cell apoptosis by using produced reactive oxygen species (ROS). In this paper, ROS-sensitive multifunctional marine biomaterial natural polysaccharide nanoparticles (CT/PTX) were designed. Aggregation-induced emission (AIE) molecules tetraphenylethylene (TPE) labeled and caffeic acid (CA) modified fucoidan (FUC) amphiphilic carrier material (CA-FUC-TK-TPE, CFTT) was fabricated, in which the thioketal bond was used as the linkage arm between TPE and fucoidan chain, giving the CFTT material ROS sensitivity. In addition, amphiphilic carrier material (FUC-TK-VE, FTVE) composed of thioketal-linked vitamin E and fucoidan was synthesized. The mixed carrier material CFTT and FTVE self-assembled in water to form nanoparticles (CT/PTX) loaded with PTX and Fe^{3+}. CT/PTX nanoparticles could induce ROS oxidative stress in tumor sites through the CDT effect induced by Fe^{3+}. The CDT effect was combined with the chemotherapeutic drug PTX to achieve tumor inhibition. In vitro cell studies have proved that CT/PTX nanoparticles have excellent cell permeability and tumor cytotoxicity. In vivo antitumor experiments confirmed effective antitumor activity and reduced side effects.

1. Introduction

Since 2001, a series of luminescent materials with aggregation-induced luminescence (AIE) properties have been developed[1–3]. Compared with the aggregation-caused quenching effect (ACQ), aggregation-induced luminescent fluorophores (AIEgens) have almost no radiation in dilute solution, but have high radiation in the aggregated state due to limited intramolecular motion[4, 5]. AIEgens have the advantages of high fluorescence efficiency, excellent optical stability, high signal-to-noise ratio, large Stokes shift, and resistance to photobleaching[6, 7]. As a type of newly developed probe, AIEgens have a wide range of medical applications[8]. Tetrastyrene (TPE) and its derivatives are the most studied AIE compounds[9].

Reactive oxygen species (ROS) play an important role in biological processes. High levels of ROS can cause oxidative damage to cellular biomolecules such as lipids, proteins, and nucleic acid molecules, leading to tumor cell death[10]. Chemodynamic therapy (CDT) is a new therapeutic strategy, which uses biochemical reactions (such as Fenton reaction and Fenton-like reaction) to produce ROS for the killing of tumor cells[11–13]. Iron-mediated Fenton reaction could convert hydrogen peroxide (H_2O_2) into highly cytotoxic hydroxyl radicals (•OH)[14].

Tumor cells proliferate abnormally fast and have a high metabolic rate[15]. The cells are in a state of oxidative stress, and the mitochondria are prone to produce excessive ROS[16]. High ROS levels have been widely used in the development of stimulus-responsive drug delivery systems. Compared with widely used intrinsic signals such as pH and GSH, ROS in tumor tissues has higher specificity[17–20]. When nanoparticles with ROS-responsive thioketal bond arrive at the tumor site with a high ROS level, the thioketal bond breaks and the nanoparticles disintegrate to release the loaded drugs, thus achieving a responsive anti-tumor effect[21, 22].

In recent years, more and more natural polysaccharides from the ocean have been developed and used in the construction and in vivo transport of nanomedicines[23]. Fucoidan is a kind of sulfurated polysaccharide, mainly composed of fucose, which can be extracted from different kinds of brown algae[24]. Fucoidan are already used in food, dietary supplements, and cosmetics[25]. Fucoidan has many biological activities, such as anti-virus, anti-inflammatory, immunomodulatory, and (anti-)angiogenic potential[26, 27]. In addition, through different mechanisms and cancer-related pathways, fucoidan was reported to have potential anticancer effects[28–30]. Because of its good hydrophilicity and biocompatibility, fucoidan has been studied and applied in drug delivery system[31].

In this study, according to the tumor microenvironment with a high ROS level, multi-functional nanoparticles based on natural marine fucoidan were designed. Caffeic acid-fucoidan-thioketal-tetraphenylethylene (CA-FUC-TK-TPE, CFTT) was successfully synthesized. In order to improve the stability of nanoparticles, adjust the particle size to the ideal range, and improve the drug loading and encapsulation efficiency, fucoidan-thioketal-vitamin E (FUC-TK-VE, FTVE) was designed and synthesized. CFTT and FTVE were mixed according to the mass ratio of 4:1 to form the composite carrier material. Through the dialysis method, paclitaxel (PTX) and the appropriate amount of $FeCl_3 \cdot 6H_2O$ were loaded into the nano-micelles formed by the composite carrier material to obtain CT/PTX. The PTX was encapsulated into the hydrophobic core of the nanomicelles; while ferric ions were chelated by CA groups through the non-covalent coordination interactions. Under the enhanced permeability and retention (EPR) effect, CT/PTX in the circulation could accumulate to the tumor site[32, 33]. After the CT/PTX nanoparticles were ingested by tumor cells, the ROS-responsive thioketal bond broke. At the same time, CT/PTX nanoparticles collapsed, releasing paclitaxel and AIEgens. Through iron-mediated Fenton reaction, nanoparticles could produce ROS at tumor sites and achieve tumor ablation in combination with chemotherapy drug paclitaxel (PTX). The synergistic generation of ROS waterfall in tumor cells by CDT effects could not only kill tumor cells, but also cause further rapid breakage of ROS sensitive bonds and promote the complete release of PTX. The results of *in vivo* and *in vitro* experiments showed that CT/PTX nanoparticles had a good effect on tumor inhibition.

2. Materials And Methods

2.1. Materials

paclitaxel (PTX), tetrahydrofuran (THF), Oxalyl chloride, 4-(*N,N*-dimethylamino)pyridine (DMAP), 1-Hydroxybenzotriazole (HOBT), 1-Ethyl-(3-dimethylaminopropyl) carbodiimide hydrochloride (EDCI), and caffeic acid (CA) were bought from Aladdin Biochemical Technology Co., Ltd. (Shanghai, China). 4-(1,2,2-triphenylethenyl)phenol (TPE-OH) was purchased from Saen Chemical Technology Co., Ltd. (Shanghai, China). Fucoidan (FUC) was purchased from Mingyue Seaweed Group Co., Ltd. (Qingdao, China). D-α-Tocopherol was purchased from Jingming Biotechnology Co., Ltd. (Beijing, China). 2,2'-[propane-2,2-diylbis(thio)]diacetic acid (TK) was purchased from Chuangyan Chemical Technology Co., Ltd. (Shanghai, China).

2.2. Synthesis of CFTT

The synthetic routes of CFTT were revealed in Fig. 1A.

First, 0.187 mM of TK was dissolved in THF, then oxaloyl chloride (0.187 mM) was slowly added at 0 ℃ [34]. After stirring at room temperature for 3 h, TK with one end of carboxyl group activated was obtained, and the system was described as solution 1. An appropriate amount of triethylamine was dropped into the THF solution of TPE-OH (0.187 mM) to obtain solution 2. Under the ice bath condition, solution 2 was slowly added into solution 1 and stirred at 55 ℃ for 6 h without light. At the end of the reaction, THF and unreacted oxaloyl chloride and triethylamine were removed using a rotary evaporator. Single-substituted TK-TPE purified products were obtained by column chromatography.

The purified TK-TPE (0.187 mM) was dissolved in formamide, then 1.5 eq of EDC and 1.5 eq of DMAP were added to activate the carboxyl group of TK-TPE at 35 ℃ for 2 h. After activation, the formamide solution of FUC was added and stirred at 35 ℃ for 48 h without light. After 48 h, the reaction solution was dialysed in deionized water for 12 h, and the deionized water was changed every 2 h. FUC-TK-TPE (FTT) was obtained by lyophilization after dialysis.

0.187 mM of CA was dissolved in formamide, then 1.2 eq of EDC and HOBT were added to activate the carboxyl group for 3 h. After the activation, the formamide solution of FTT was added into the activated CA reaction solution, and the reaction was stirred at room temperature without light for 48 h. After the reaction, CA-FUC-TK-TPE (CFTT) was obtained by dialysis and freeze-drying. ^{1}H-NMR was used to verify the structure of CFTT.

2.3. Synthesis of FTVE

The synthetic route of FTVE was shown in Fig. 1B.

After one end of the carboxyl group of TK was activated by the acyl chloride method, THF solution containing 80.54 mg of D-α-tocopherol (VE) was slowly added under ice bath condition, and a small amount of triethylamine was injected at the same time. After stirring at 55 ℃ for 6 h, the reaction solution was rotated to remove volatile components. Pure VE-TK was obtained by column chromatography. After activation at room temperature for 2 h, the formamide solution of FUC was added and reacted at 35 ℃ for 36 h. Finally, FUC-TK-VE (FTVE) was obtained through dialysis and lyophilization. ^{1}H-NMR was used to verify the structure of FTVE.

2.4. Preparation of CT/PTX nanoparticles

8 mg of CFTT and 2 mg of FTVE were dissolved in 4 mL of formamide, and then PTX (1 mg/mL) was slowly and successively added into the carrier material solution. After the solution was mixed evenly by ultrasound, the solution was dialysed in the 2000 Da dialysis bag for 10 h, and appropriate $FeCl_3 \cdot 6H_2O$ was added for further dialysis. After dialysis, CT/PTX was obtained through 0.22μm membrane filtration.

2.5. Characterizations

The particle size and polydispersity index (PDI) of CT/PTX were determined by Delsa Nano C Particle Analyzer[35]. TEM was used to observe the morphology of CT/PTX nanoparticles. The content of PTX was determined by HPLC at 227 nm[36]. The DL% were calculated as follows:

DL% = weight of drugs in nanoparticles / weight of nanoparticles × 100%

2.6. In vitro ROS- responsive assay

1 mL of concentrated CT/PTX nanoparticles solution was packed into dialysis bags of 2000 Da respectively. These dialysis bags were put into centrifuge tubes containing 47 mL PBS (pH 7.4, containing 0.5% Tween 80) with different concentrations of H_2O_2 (0, 0.1, 1, and 10 mM). The samples were incubated on a thermostatic water bath shaker at 37°C. At different time points specified, 1.0 mL of the release medium was collected, and 1.0 mL of fresh release medium was subsequently added to keep the medium volume constant. The concentration of PTX in the collected release medium was determined by HPLC.

In order to prove that CT/PTX nanoparticles could induce Fenton reaction to produce ROS, methylene blue (MB) was used to study Fenton catalytic activity of CT/PTX nanoparticles in the presence of H_2O_2[11]. •OH can degrade MB, and the absorbance value of MB at 664 nm decreases, which indirectly reflects the formation of •OH. Compared with MB alone and MB containing H_2O_2, the changes of absorbance values at 664 nm were recorded after 3 h co-incubation with MB, H_2O_2, and CT/PTX nanoparticles.

2.7. In vitro cytotoxicity assays

FT/PTX and CT/PTX nanoparticles were prepared by the dialysis method. Different from the preparation of CT/PTX, the carrier material of FT/PTX is a mixture of FTT and FTVE, and the mass ratio of FTT to FTVE is 4:1. The cytotoxicity of CT/PTX and FT/PTX nanoparticles against A549 was determined by MTT assay[37, 38]. A549 cells were respectively plated in 96-well plates. After incubation for 24 h, the old culture medium was discarded, and a fresh complete culture medium containing different preparations (Free PTX, FT/PTX, CT/PTX) was added. After incubation for 24 h or 48 h, the cells were incubated with MTT solution for 4 h. Then, DMSO was added to dissolve the violet formazan crystals. Finally, the absorbance was measured at 490 nm using a microplate reader.

2.8. Cellular uptake and distribution

A549 cells and B16F10 cells were incubated in a 24-well plate for 24 h. When the cells adhered to the wall, CT/PTX at a dose of 10 μg mL^{-1} (PTX) were added and incubated for 1 h. After washing and fixing, cell images were obtained with an inverted fluorescent microscope to observe the cellular uptake.

2.9. ROS detection assay

The ROS generation capacities of Free TPE-OH, FT/PTX and CT/PTX were evaluated by DCFDA, which is non-fluorescent however transformed into DCF with green fluorescence in the presence of ROS[39, 40].

The A549 cells were incubated in a 6-well plate and treated with FT/PTX and CT/PTX (Fe^{3+}concentration: 8 μg/mL) for 5 h. After incubation, an appropriate amount of DCFDA working solution was used to detect the ROS generation.

2.10. In vivo distribution and imaging

0.2 mL of Free DiR, FT/DiR and CT/DiR were delivered into nude mice bearing A549 tumors by caudal vein injection when the tumor had grown to an appropriate size. At different time points (2, 4, 8, 12, 24 h), and in vivo fluorescence imaging system was used to monitor the distribution of fluorescence in the body of the tumor-bearing nude mice.

2.11. In vivo antitumor efficiency and histological analysis

The nude mice bearing A549 tumors were randomly divided into four groups, including saline, Free PTX, FT/PTX, and CT/PTX. The A549 tumor-bearing nude mice were intravenously injected with different PTX preparations (PTX dosage: 10 mg/kg) every three days. The tumor volume and bodyweight of the nude mice were measured and recorded before each administration. After the nude mice were humanely sacrificed, major organs and tumors were collected and preserved in 4% paraformaldehyde solution quickly. Hematoxylin and eosin (H&E) staining assay was conducted to study the anti-tumor effect of different PTX preparations. The expression of bcl-2 and MMP-9 in tumor tissues was investigated by immunohistochemistry assay to explore the mechanism of tumor cell apoptosis.

3. Results And Discussion

3.1. Characterization of CFTT and FTVE

The ^{1}H-NMR spectrum of CFTT was shown in Fig. 2A. In the ^{1}H-NMR spectrum of FUC, the signal peak at 1.23 ppm is the -CH_3 signal peak of FUC. In the FTT spectrum, the peaks at a (δ6.70 ppm) and b (δ6.45 ppm) were the characteristic peaks of the proton from the TPE-O benzene ring; the peak at c (δ2.74 ppm) corresponded to the -CH_2- of TK, and the typical signal of FUC was observed at 1.2 ppm. The above results indicated that TPE-OH was successfully connected to the FUC chain through the TK bond. In the ^{1}H-NMR spectrum of CFTT, in addition to the FTT-related characteristic peaks, new characteristic peaks appeared in the range of 6.1–6.3 ppm were the signals of CA, confirmed that CFTT was successfully obtained.

The ^{1}H-NMR spectrum of FTVE was shown in Fig. 2B. FTVE presented chemical shifts located at approximately 8.3 ppm (a) and 2.7 ppm (b), which were typical signals of D-α-tocopherol (the ‘H’ of benzene ring) and TK (-CH_2-), respectively. The above results all proved that FTVE was successfully synthesized.

3.2. Characterization of CT/PTX nanoparticles

The particle hydrodynamic diameter distribution, Zeta potential and the TEM image of CT/PTX were shown in Fig. 3. The particle size of CT/PTX nanoparticles was 150.3 ± 12.0 nm, and the polydispersity index (PDI) was 0.098 ± 0.029, indicating the excellent uniformity of the nanoparticles. TEM images (Fig. 3B) showed that the nanoparticles were spherical. The DL% of PTX in the nanoparticles was 5.80 ± 0.91%.

3.3. In vitro ROS- responsive assay

The in vitro PTX release characteristics of CT/PTX nanomicelles at different H_2O_2 concentrations were shown in Fig. 4A. When the concentration of H_2O_2 was 0 mM, almost no ROS was produced. The core-shell structure of CT/PTX is relatively stable, and the PTX release is slow, which is beneficial to avoid the release of PTX in normal tissues and reduce the side effects. It could be observed that with the increase of H_2O_2 concentration in the release medium, the cumulative release of PTX also increased gradually. These results indicated that the PTX release of CT/PTX nanomicelles was concentration (ROS) dependent.

As shown in Fig. 4B, when CT/PTX nanoparticles and H_2O_2 were incubated with MB for 3h, the absorbance of MB decreased significantly, indicating the production of •OH indirectly. However, no significant decrease in absorbance of MB was found when MB was treated with H_2O_2 alone. The results showed that Fe^{3+} in CT/PTX nanoparticles could be used as Fenton reaction catalyst-like to produce ROS.

3.4. In vitro cytotoxicity assays

The toxicity of Free PTX, FT/PTX and CT/PTX to A549 cells was investigated (Fig. 5A,B). It could be observed that the activity of A549 cells changed with the increase of PTX concentration in different preparations. Compared with the FT/PTX group, the CT/PTX group showed stronger cell inhibition after 48 h incubation, indicating that CT/PTX produced cytotoxic ROS through the CDT effect. The free PTX group showed strong cytotoxicity, which may be attributed to the inhibitory effect of organic solvents added in the preparation of Free PTX.

The toxicity of CFTT/FTVE material to A549 cells was shown in Fig. 5C. When the treatment time was 24 h, the inhibitory effect of CFTT/FTVE material on A549 cells was not obvious. After 48 h treatment, with the increase of the concentration of CFTT/FTVE material, the cell survival rate decreased slightly and showed low toxicity, which may be attributed to the potential anti-tumor effect of fucoidan.

3.5. Cellular uptake and distribution

The cellular uptake of CT/PTX in the A549 cells and B16F10 cells were observed with an inverted fluorescence microscope. According to Fig. 6, after incubation with the cells for 1 h, the blue fluorescence of the CT/PTX appeared in the cytoplasm, suggesting that the nanoparticles could be rapidly endocytosed.

3.6. ROS detection assay

The stronger the green fluorescence intensity in A549 cells treated with DCFDA, the more ROS were generated in the cells. According to Fig. 7, compared with the control and FT/PTX group, the CT/PTX group had the strongest green fluorescence intensity, indicating that CT/PTX nanoparticles produced a large amount of intracellular ROS under the effect of CDT.

3.7. In vivo distribution and imaging

In vivo real-time fluorescence imaging of Free DiR, FT/DiR, and CT/DiR was shown in Fig. 8A. In the Free DiR group, DiR was mainly distributed in the liver, and there was almost no DiR accumulation in the tumor site. Compared with the Free DiR group, the DiR fluorescence intensity of FT/DiR and CT/DiR group increased gradually at the tumor site over time, indicating accumulation of nanoparticles at the tumor site.

Fluorescent imaging of isolated tissues (Fig. 8B) showed that DiR fluorescence was observed in the FT/DiR and CT/DiR groups at the tumor site, indicating that nanoparticles could accumulate at the tumor site effectively through the EPR effect, which was consistent with the results of in vivo imaging in nude mice.

3.8. In vivo safety evaluation

It was worth noting that there was no significant difference in the change of body weight (Fig. 9A) and no obvious tissue and organ damage (Fig. 9B) of nude mice within a short period of administration, indicating that the designed multi-functional CT/PTX nanoparticles based on marine polysaccharides had satisfactory safety.

3.9. In vivo antitumor efficiency and histological analysis

As shown in Fig. 10A, the tumor inhibition effect of the Free PTX group was unsatisfactory. Different from the tumor site accumulation characteristics and blood circulation stability of nanoparticles, Free PTX rarely accumulated at the tumor site, leading to poor therapeutic effect. Results showed that the antitumor effect of CT/PTX was more obvious than that of FT/PTX, which indicated that treatment with PTX and CDT was effective.

The results of the H&E staining assay of tumors was shown in Fig. 10B. Tumor cells in the saline group were closely arranged and normal in shape. The morphology of tumor cells in the PTX group was not significantly changed, but the density of tumor cells was slightly decreased compared with the saline group. In the CT/PTX group, loose cells, abnormal cell morphology, and damaged nuclei were observed, indicating its surprising anti-tumor effect in vivo.

The high expression of bcl-2 can slow down the apoptosis of tumor cells and promote the development of drug resistance. In immunohistochemistry, when bcl-2 was positively expressed in tumor cells, brownish yellow granules appeared in the cytoplasm. As observed in Fig. 10C, the obvious brown color appeared in the tumor cytoplasm of the saline and Free PTX group, suggesting the strong expression of

bcl-2. The brown-yellow color of tumor cytoplasm was the weakest in the CT/PTX group, indicating that the expression of bcl-2 in tumor cells was rapidly down-regulated after administration.

MMP-9 promotes the growth and metastasis of tumors. When MMP-9 is positively expressed in tumor cells, the cytoplasm and membrane of tumor cells appear brownish yellow granules. In Fig. 10D, compared with the saline and Free PTX groups, the tumor cells in the CT/PTX group showed a weaker brown-yellow color, which indirectly reflected less MMP-9 positive expression, indicating that the CT/PTX group effectively inhibited the invasion and metastasis of the tumor.

4. Conclusion

- We designed and constructed a type of novel ROS-responsive nanomedicine based on marine fucoidan by combining PTX chemotherapy and CDT. The formed CT/PTX nanoparticles have the appropriate particle size, spherical structure, surface charge and drug loading capacity. The ROS-sensitivity of CT/PTX was demonstrated by an in vitro release assay. In vitro cell uptake experiments showed that the CT/PTX could be rapidly endocytosed. MTT assays showed that CT/PTX nanoparticles had an obvious inhibitory effect on the tumor cell. ROS detection experiments indicated that CT/PTX nanoparticles could form ROS waterfall after entering into tumor cells. In vivo studies have shown that CT/PTX nanoparticles exhibited reduced side effects, enhanced tumor accumulation and improved anticancer activity. Overall, this study provides a promising strategy for developing marine polysaccharide-based nanomedicines with satisfactory anticancer effects and security.

Declarations

Acknowledgements

This study was financially supported by Taishan Scholar Foundation of Shandong Province (No.qnts20161035); Natural Science Foundation of Shandong Province (No.ZR2019ZD24, ZR2019YQ30); Graduate Innovation Foundation of Yantai University, GIFYTU.

Authors' contributions

CG, XL and QC conceived of this study and designed it. DQC contributed to data collection and article writing. MK performed the preparation of the references in the manuscript. All authors read and approved the final manuscript.

Funding

This funding was supported by Taishan Scholar Foundation of Shandong Province (No.qnts20161035); Natural Science Foundation of Shandong Province (No. ZR2019ZD24,ZR2019YQ30).

Availability of data and materials

All data generated or analyzed in this study are included in this article.

Ethics approval and consent to participate

All procedures involving laboratory animals are performed in accordance with the ethics committee guidelines at the Ocean University of China and Yantai University.

Consent for publication

Not applicable.

Competing interests

The authors declare no conflict of interest in this article.

Author details

[1]College of Marine Life Science, Ocean University of China, Qingdao, 266003,PR China; [2]Collaborative Innovation Center of Advanced Drug Delivery System and Biotech Drugs, School of Pharmacy, Yantai University, Yantai, 264005,PR China.

References

1. Gu X, Kwok R, Lam J, Tang B. AIEgens for biological process monitoring and disease theranostics. Biomaterials.2017;146:115-135.
2. Cheng Y, Huang FJ, Min XH, Gao PC, Zhang TC, Li XC, Liu BF, Hong YN, Lou XD, Xia F. Correction to Protease-Responsive Prodrug with Aggregation-Induced Emission Probe for Controlled Drug Delivery and Drug Release Tracking in Living Cells. Analytical chemistry. 2016;88(17):8913-9.
3. Dong ZZ, Bi YZ, Cui HR, Wang YD, Wang CL, Li Y, Jin HW, Wang CQ. AIE Supramolecular Assembly with FRET Effect for Visualizing Drug Delivery. ACS applied materials & interfaces. 2019;11(27):23840-23847.
4. Gao M, Tang BZ. Aggregation-induced emission probes for cancer theranostics.Drug Discov Today. 2017;22(9):1288-1294.
5. Dai J, Wu X, Ding SY, Lou XD, Xia F, Wang SX, Hong YN. Aggregation-Induced Emission Photosensitizers: From Molecular Design to Photodynamic Therapy. Journal of medicinal chemistry. 2020;63(5):1996-2012.
6. Gao M, Chen JJ, Lin GW, Li SW, Wang L, Qin AJ, Zhao ZJ, Ren L, Wang YJ, Tang BZ. Long-Term Tracking of the Osteogenic Differentiation of Mouse BMSCs by Aggregation-Induced Emission Nanoparticles. ACS applied materials & interfaces. 2016;8(28):17878-84.
7. Zhang WJ, Kwok RT, Chen YL, Chen SJ, Zhao EG, Yu CY, Lam JW , Zheng QC, Tang BZ. Real-time monitoring of the mitophagy process by a photostable fluorescent mitochondrion-specific bioprobe with AIE characteristics. Chem Commun (Camb). 2015;51(43):9022-5.

8. Yao HM, Dai J, Zhuang ZY, Yao JY, Wu ZX, Wang SX, Xia F, Zhou J, Lou XD, Zhao ZJ. Red AIE conjugated polyelectrolytes for long-term tracing and image-guided photodynamic therapy of tumors.Science China Chemistry. 2020;63(12):1815-1824.
9. La DD, Anuradha A, Hundal AK, Bhosale SV, Jones LA, Bhosale SV. pH-Dependent self-assembly of water-soluble sulfonate-tetraphenylethylene with aggregation-induced emission.Supramolecular Chemistry. 2017;30(1): 1-8.
10. Wang S, Yu GC, Wang ZT, Jacobson O, Lin LS, Yang WJ, Deng HZ, He ZM, Liu Y, Chen ZY, Chen XY. Enhanced Antitumor Efficacy by a Cascade of Reactive Oxygen Species Generation and Drug Release. Angew Chem Int Ed Engl. 2019;58(41) :14758-14763.
11. Guo Y, Zhang X, Sun W, Jia HR, Zhu YX, Zhang X, Zhou N, Wu FG. Metal–Phenolic Network-Based Nanocomplexes that Evoke Ferroptosis by Apoptosis: Promoted Nuclear Drug Influx and Reversed Drug Resistance of Cancer. Chemistry of Materials. 2019; 31(24) :10071-10084.
12. Qin L, Wang ZH, Fu YK, Lai C, Liu XG, Li BS, Liu SY, Yi H, Li L, Zhang MM, Li ZW, Cao WC, Niu QY. Gold nanoparticles-modified MnFe2O4 with synergistic catalysis for photo-Fenton degradation of tetracycline under neutral pH. Journal of Hazardous Materials. 2021;414 :125448.
13. Zhao P, Tang Z, Chen X, He Z, He X, Zhang M, Liu Y, Ren D, Zhao K, Bu W. Ferrous-cysteine–phosphotungstate nanoagent with neutral pH fenton reaction activity for enhanced cancer chemodynamic therapy. Materials Horizons. 2019; 6(2) : 369-374.
14. Dong ZL, Feng LZ, Chao Y, Hao Y, Chen MC, Gong F, Han X, Zhang R, Cheng L, Liu Z. Amplification of Tumor Oxidative Stresses with Liposomal Fenton Catalyst and Glutathione Inhibitor for Enhanced Cancer Chemotherapy and Radiotherapy. Nano Lett. 2019; 19(2) :805-815.
15. Uthaman S, Huh KM, Park IK. Tumor microenvironment-responsive nanoparticles for cancer theragnostic applications. Biomater Res. 2018;22(46) :22.
16. Kim YS, Kim S, Kang HC, Shim MS. ROS-responsive thioether-based nanocarriers for efficient pro-oxidant cancer therapy. Journal of Industrial and Engineering Chemistry. 2019;75 :238-245.
17. Lv XM, Zhu YY, Ghandehari H, Yu A, Wang YJ. An ROS-responsive and self-accelerating drug release nanoplatform for overcoming multidrug resistance. Chem Commun (Camb). 2019; 55(23):3383-3386.
18. Yin W, Ke WD, Chen WJ, Xi LC, Zhou QH, Mukerabigwi JF, Ge Z. Integrated block copolymer prodrug nanoparticles for combination of tumor oxidative stress amplification and ROS-responsive drug release. Biomaterials. 2019; 195: 63-74.
19. Priya Dharshini K, Fang H, Ramya Devi D, Yang JX, Luo RH, Zheng YT, Brzezinski M, Vedha Hari BN. pH-sensitive chitosan nanoparticles loaded with dolutegravir as milk and food admixture for paediatric anti-HIV therapy. Carbohydr Polym. 2021; 256 :117440.
20. Fu DJ, Ni Z, Wu KR, Cheng P, Ji XF, Li GY, Shang XF. A novel redox-responsive ursolic acid polymeric prodrug delivery system for osteosarcoma therapy. Drug delivery. 2021;28(1) :195-205.
21. Li YJ, Hu J, Liu X, Liu Y, Lv SX, Dang JJ, Ji Y, He JJ, Yin LC. Photodynamic therapy-triggered on-demand drug release from ROS-responsive core-cross-linked micelles toward synergistic anti-cancer

treatment. Nano Research. 2019; 12(5):999-1008.

22. Xu L, Zhao MY, Zhang H, Gao WX, Guo ZY, Zhang XQ, Zhang JF, Cao J, Pu YJ, He B. Cinnamaldehyde-Based Poly(ester-thioacetal) To Generate Reactive Oxygen Species for Fabricating Reactive Oxygen Species-Responsive Nanoparticles. Biomacromolecules. 2018;19(12):4658-4667.
23. Yu YM, Zou SH, Wang KL, Liang RC, Fan XX, Wang BJ, Liu MN, Fang L, Liu WH, Wu ZM, Chen DQ. Synthesis, Characterization and In Vitro Evaluation of Dual pH/Redox Sensitive Marine Laminarin-Based Nanomedicine Carrier Biomaterial for Cancer Therapy. J Biomed Nanotechnol. 2018; 14(9) :1568-1577.
24. Oliveira C, Neves NM, Reis RL, Martins A, Silva TH. A review on fucoidan antitumor strategies: From a biological active agent to a structural component of fucoidan-based systems. Carbohydr Polym. 2020; 239:116131.
25. Zayed A, El-Aasr M, Ibrahim AS, Ulber R. Fucoidan Characterization: Determination of Purity and Physicochemical and Chemical Properties. Mar Drugs. 2020;18(11) .
26. Fitton JH, Park AY, Karpiniec SS, Stringer DN. Fucoidan and Lung Function: Value in Viral Infection. Mar Drugs.2020; 19(1).
27. Hsu HY, Lin TY, Hu CH, Shu DTF, Lu MK. Fucoidan upregulates TLR4/CHOP-mediated caspase-3 and PARP activation to enhance cisplatin-induced cytotoxicity in human lung cancer cells. Cancer Lett. 2018;432:112-120.
28. Etman SM, Abdallah OY, Elnaggar YSR. Novel fucoidan based bioactive targeted nanoparticles from Undaria Pinnatifida for treatment of pancreatic cancer. Int J Biol Macromol. 2020; 145:390-401.
29. Hsu HY, Lin TY, Lu MK, Leng PJ, Tsao SM, Wu YC. Fucoidan induces Toll-like receptor 4-regulated reactive oxygen species and promotes endoplasmic reticulum stress-mediated apoptosis in lung cancer. Sci Rep. 2017;7:44990.
30. Ale MT, Maruyama H, Tamauchi H, Mikkelsen JD, Meyer AS. Fucoidan from Sargassum sp. and Fucus vesiculosus reduces cell viability of lung carcinoma and melanoma cells in vitro and activates natural killer cells in mice in vivo. Int J Biol Macromol. 2011.49(3):331-6.
31. Amaral AJR, Gaspar VM, Mano JF. Responsive laminarin-boronic acid self-healing hydrogels for biomedical applications. Polymer Journal. 2020;52(8):997-1006.
32. Zhou Q, Zhang L, Yang TH, Wu H. Stimuli-responsive polymeric micelles for drug delivery and cancer therapy. Int J Nanomedicine. 2018; 13:2921-2942.
33. Ke XY, Ng VW, Ono RJ, Chan JM, Krishnamurthy S, Wang Y, Hedrick JL, Yang YY. Role of non-covalent and covalent interactions in cargo loading capacity and stability of polymeric micelles. J Control Release. 2014; 193:9-26.
34. Wang KL, Guo CJ, Zou SH, Yu YM, Fan XX, Wang BJ, Liu MN, Fang L, Chen DQ. Synthesis, characterization and in vitro/in vivo evaluation of novel reduction-sensitive hybrid nano-echinus-like nanomedicine. Artif Cells Nanomed Biotechnol. 2018; 46:659-667.
35. Wang BJ, Zhang W, Zhou XD, Liu MN, Hou XY, Cheng ZT, Chen DQ. Development of dual-targeted nano-dandelion based on an oligomeric hyaluronic acid polymer targeting tumor-associated

macrophages for combination therapy of non-small cell lung cancer. Drug Deliv. 2019; 26(1):1265-1279.

36. Zhang X, Liang N, Gong XF, Kawashima Y, Cui FD, Sun SP. Tumor-targeting micelles based on folic acid and alpha-tocopherol succinate conjugated hyaluronic acid for paclitaxel delivery. Colloids Surf B Biointerfaces. 2019; 177: 11-18.
37. Fang L, Lin H, Wu ZF, Wang Z, Fan XX, Cheng ZT, Hou XY, Chen DQ. In vitro/vivo evaluation of novel mitochondrial targeting charge-reversal polysaccharide-based antitumor nanoparticle. Carbohydr Polym. 2020;234:115930.
38. Xiang JJ, Li YW, Zhang YF, Wang GW, Xu HX, Zhou ZX, Tang JB, Shen YQ. Polyphenol-cisplatin complexation forming core-shell nanoparticles with improved tumor accumulation and dual-responsive drug release for enhanced cancer chemotherapy. J Control Release. 2021; 330:992-1003.
39. Li J, Ni X, Zhang JT, Liang Y, Gao ZY, Zhang XY, Zheng DH, Ding D. A fluorescence and photoactivity dual-activatable prodrug with self-synergistic magnification of the anticancer effect. Materials Chemistry Frontiers. 2019; 3(7):1349-1356.
40. Zhen SJ, Yi XQ, Zhao ZJ, Lou XD, Xia F, Tang BZ. Drug delivery micelles with efficient near-infrared photosensitizer for combined image-guided photodynamic therapy and chemotherapy of drug-resistant cancer. Biomaterials. 2019; 218:119330.

Figures

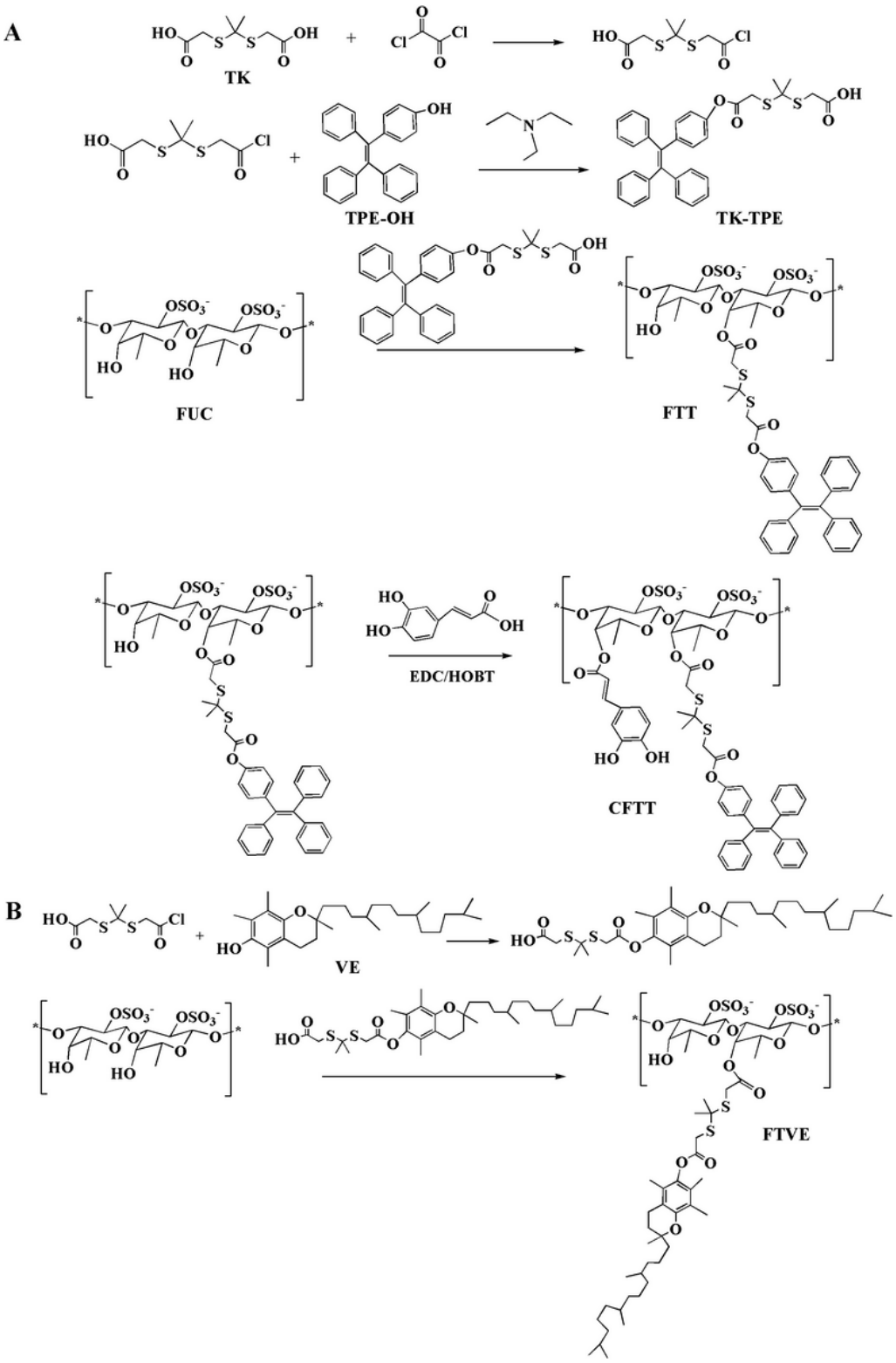

Figure 1

Synthetic routes of CFTT (A) and FTVE (B).

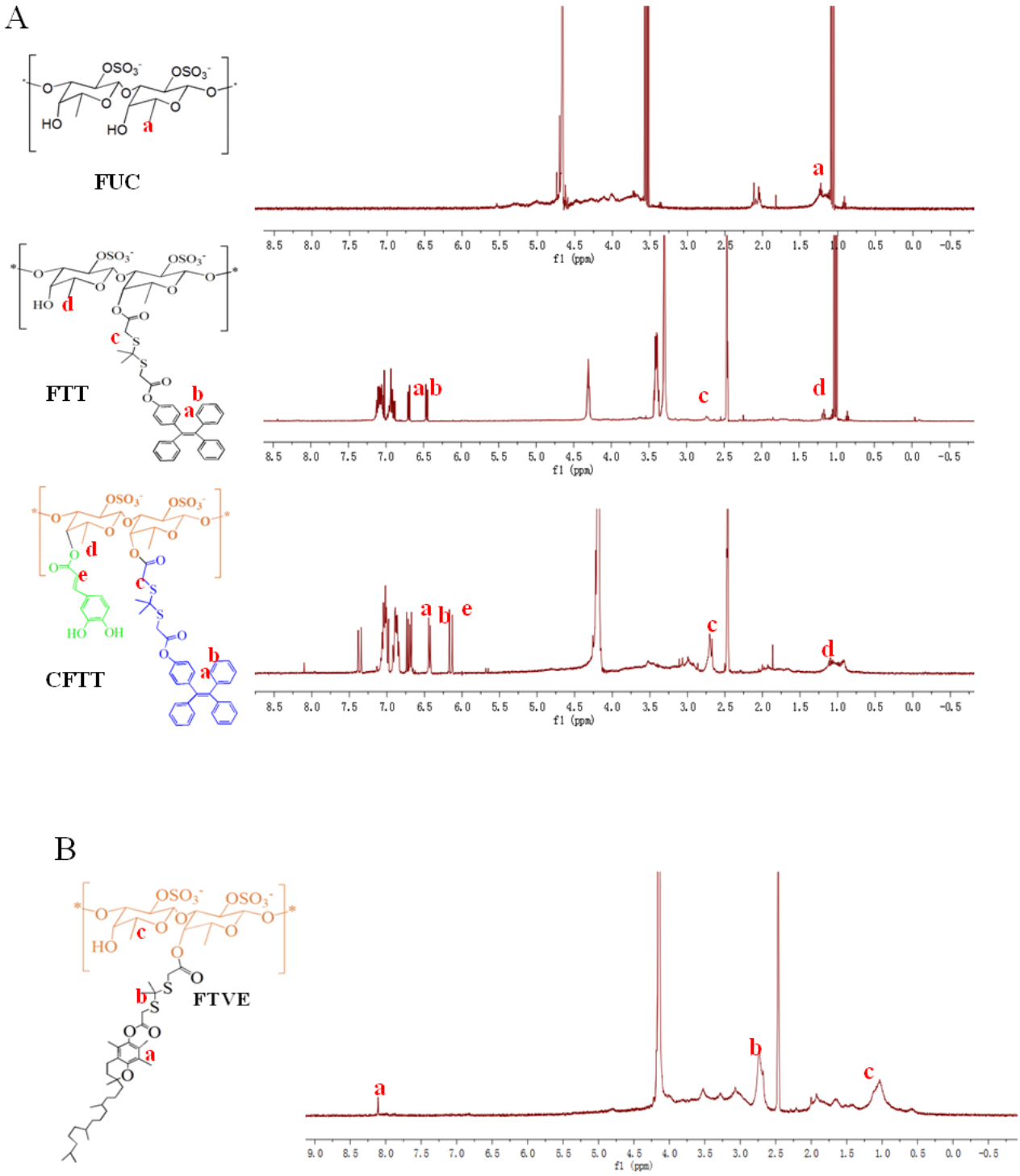

Figure 2

The 1H-NMR spectra of CFTT (A) and FTVE (B).

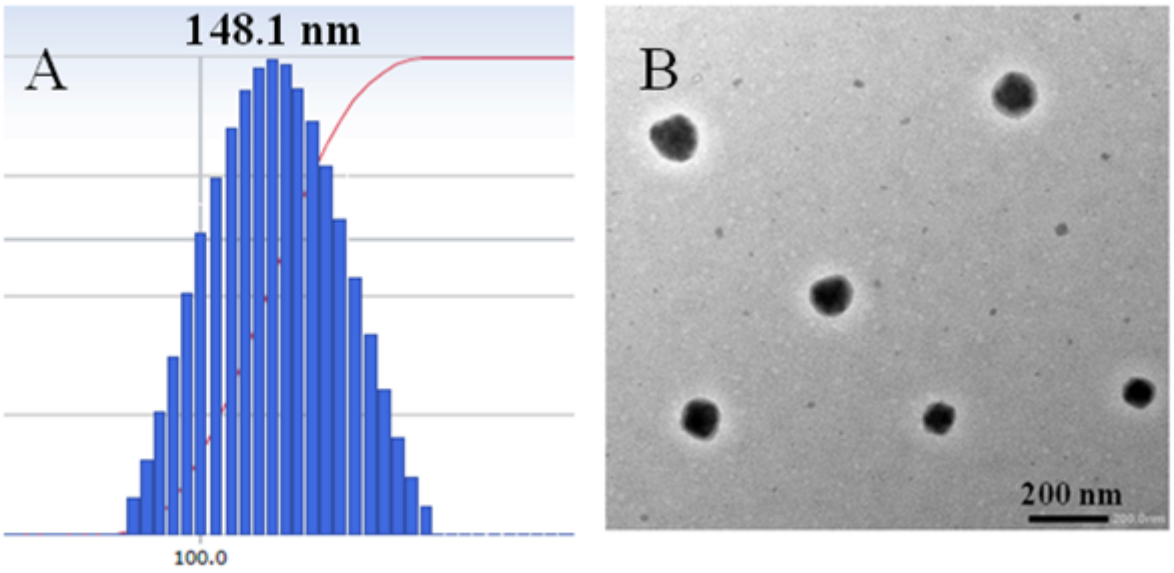

Figure 3

Characterization of CT/PTX nanoparticles: Diameter distribution (A) and TEM image (B)

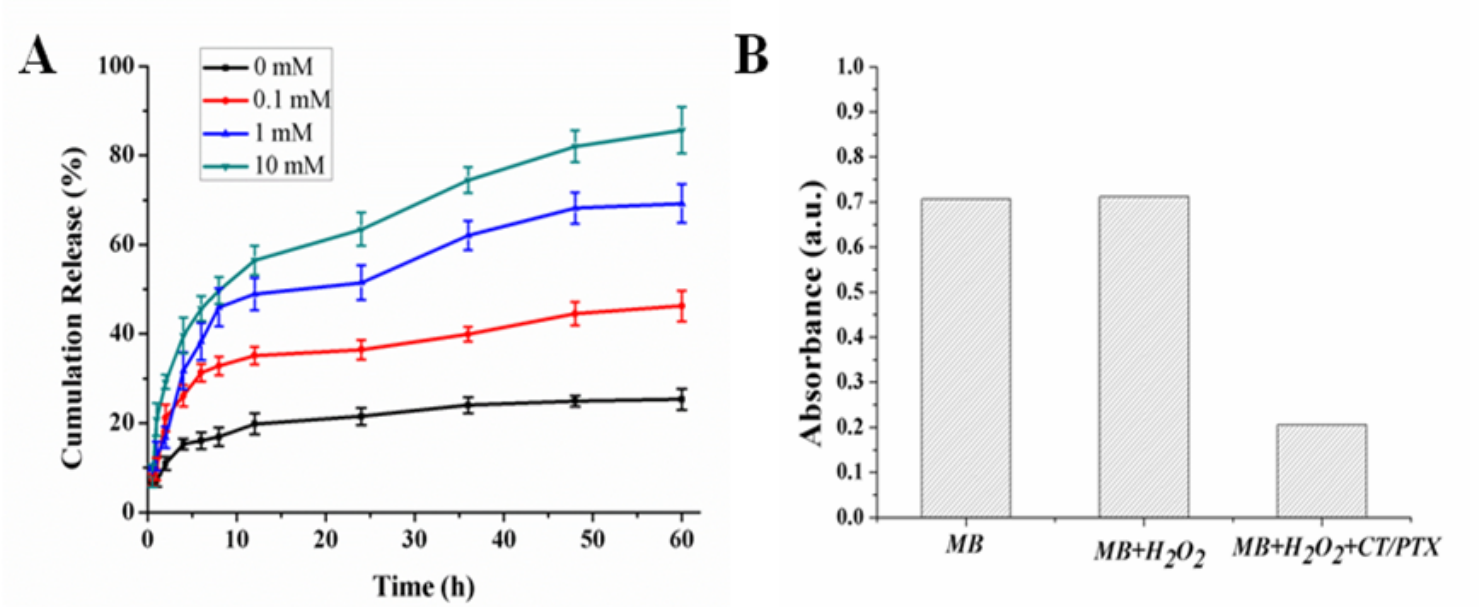

Figure 4

In vitro investigation of CT/PTX nanoparticles: ROS-sensitive PTX release characteristic of CT/PTX (n=3) (A) and MB degradation triggered by Fenton reaction (B).

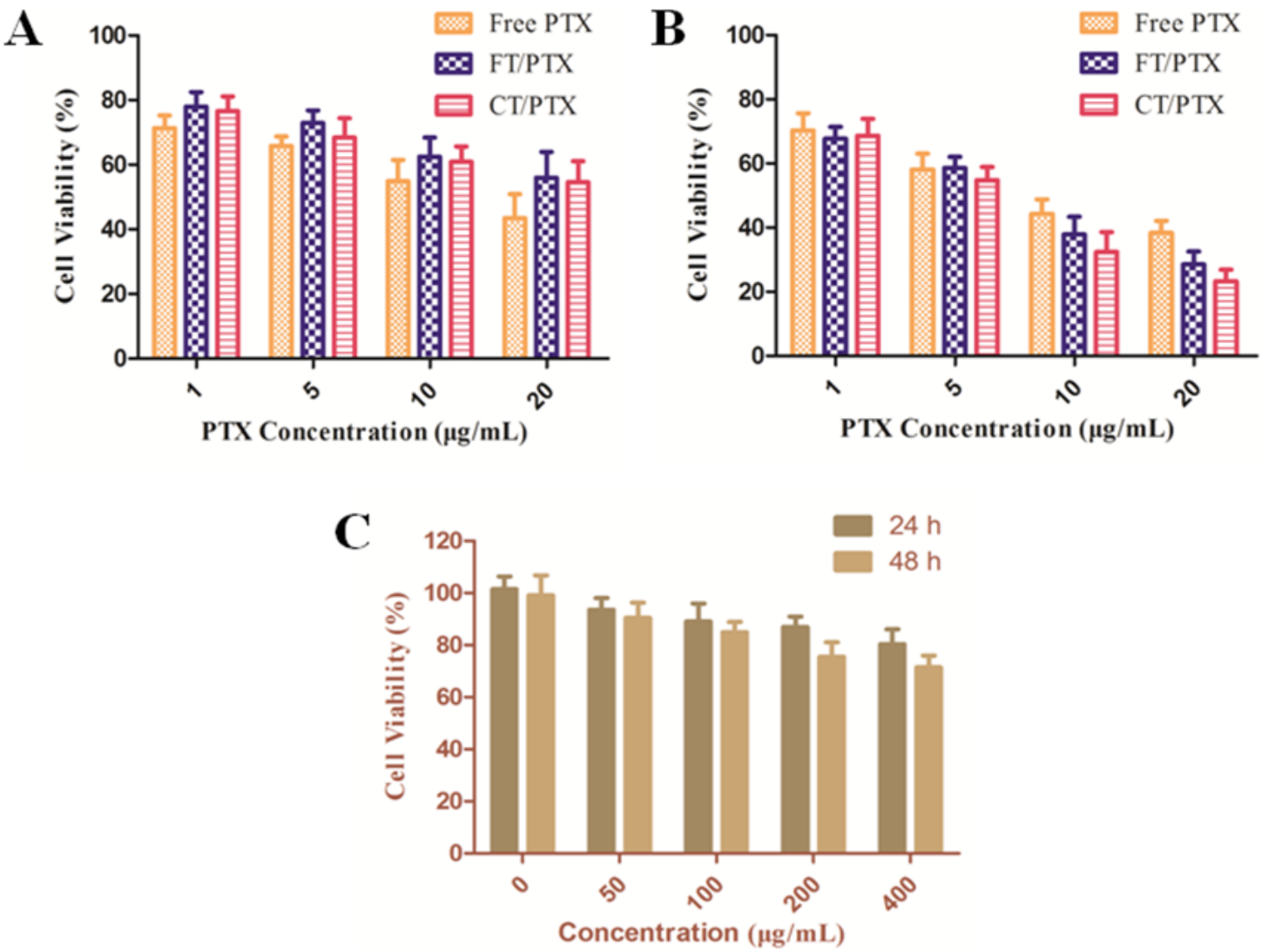

Figure 5

Cytotoxicity of PTX, FT/PTX and CT/PTX against A549 cells after 24 h (A) and 48 h (B); Cytotoxicity of CFTT/FTVE (C) against A549 cells. The data are means±SD (n = 3).

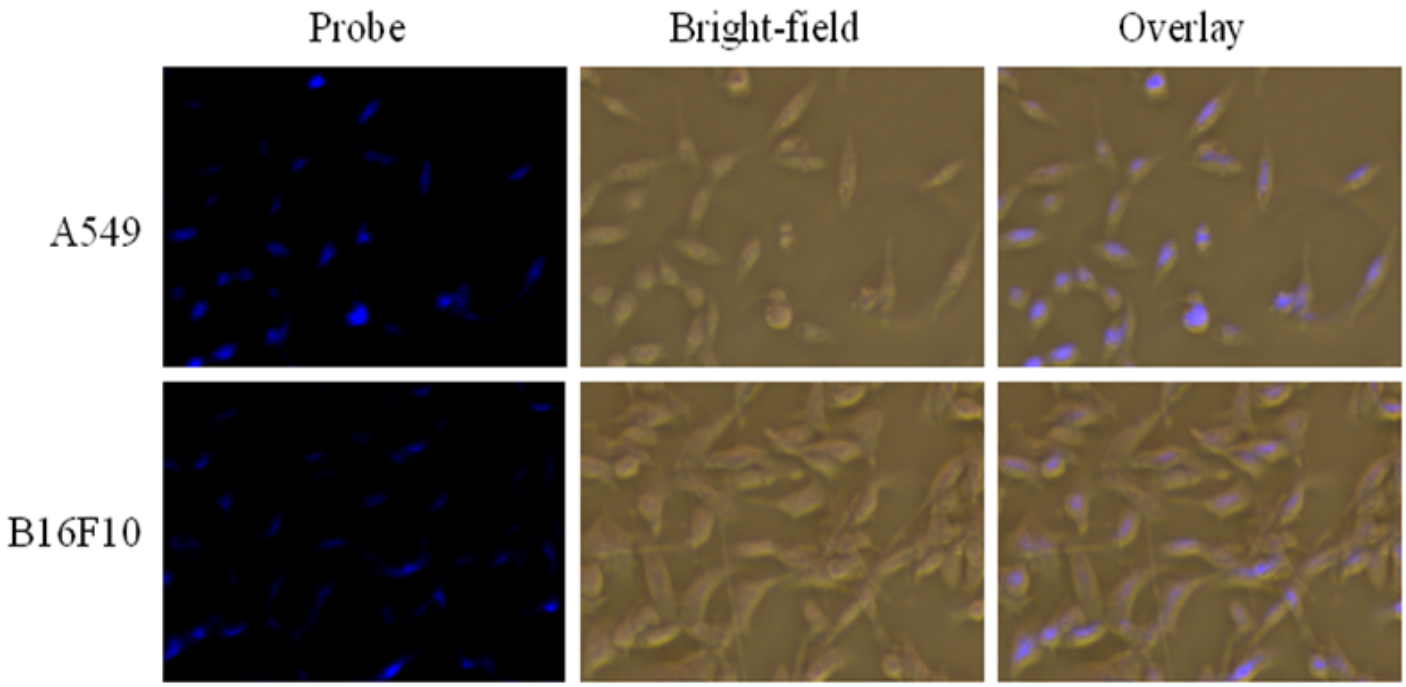

Figure 6

CLSM images of A549 cells (A) and B16F10 cells (B) after incubation with CT/PTX for 1 h.

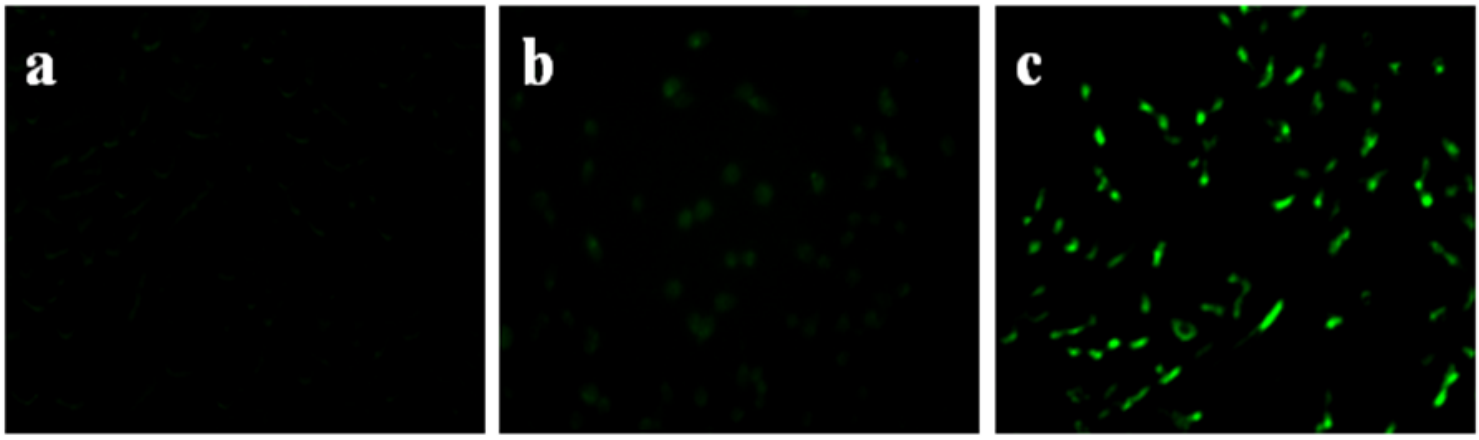

Figure 7

ROS generation: (A) Control, (B) FT/PTX and (C) CT/PTX.

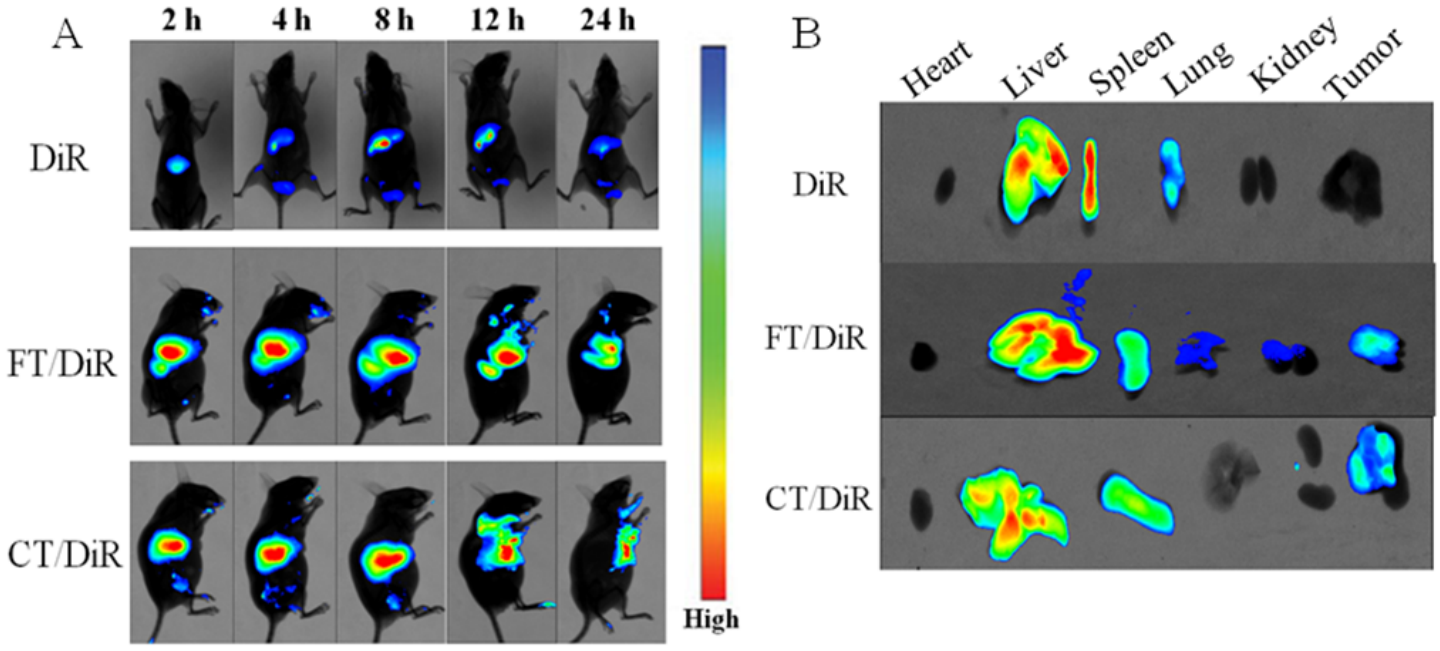

Figure 8

The real-time fluorescence imaging of tumor-bearing nude mice (A) and anatomical organs and tumors (B).

Figure 9

Evaluation of in vivo safety: (A) The body change of tumor-bearing nude mice. (B) H&E staining of main organs of different groups: (a) saline, (b) Free PTX, (c) FT/PTX, (d) CT/PTX.

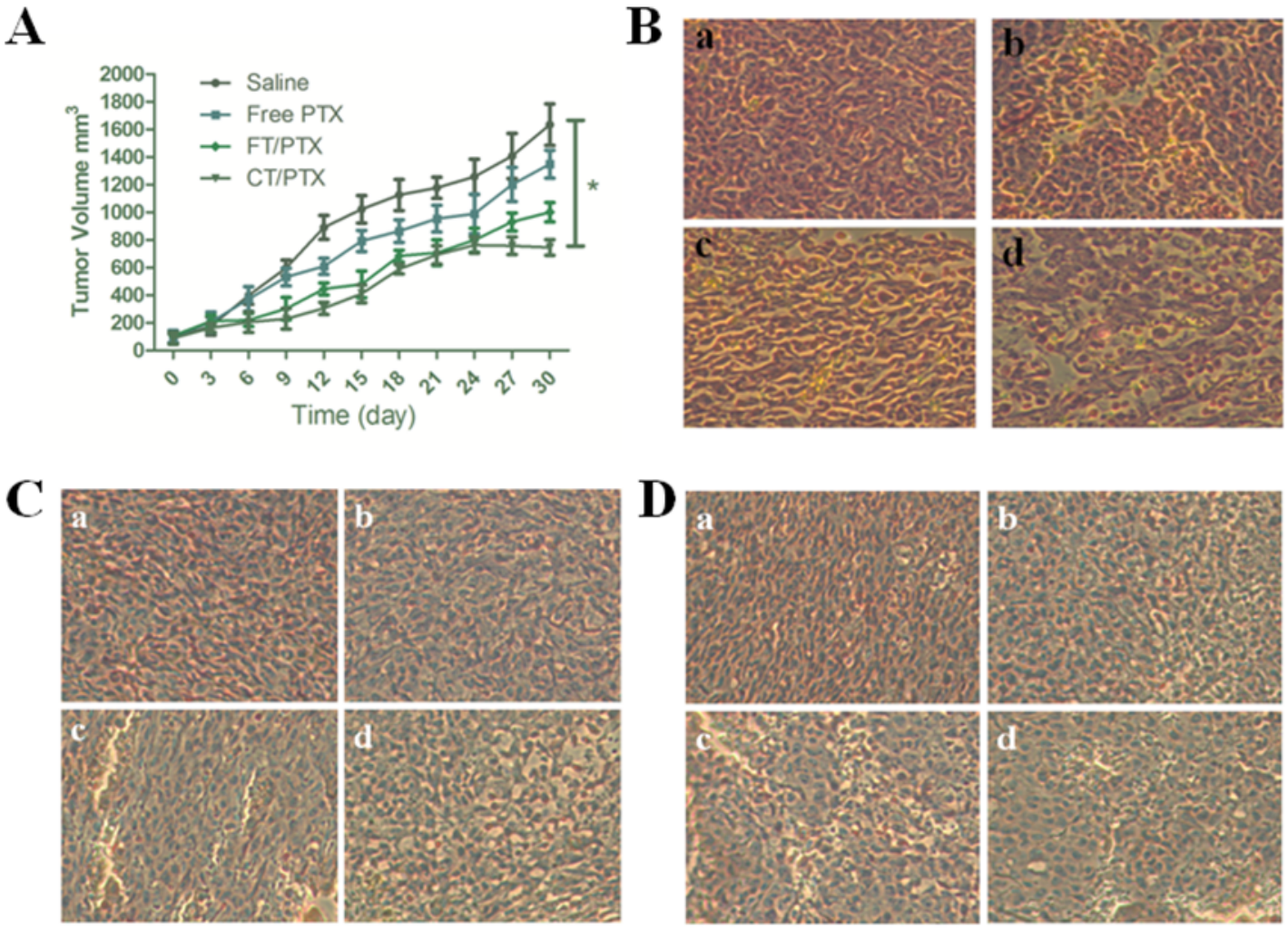

Figure 10

In vivo antitumor efficiency and histological analysis: (A) Tumor volume changes of nude mice (*P<0.05); (B) H&E staining of tumor tissues: (a) saline, (b) Free PTX, (c) FT/PTX, (d) CT/PTX; Bcl-2 (C) and MMP-9 (D) expression in tumor tissues: (a) saline, (b) Free PTX, (c) FT/PTX, (d) CT/PTX.

Supplementary Files

This is a list of supplementary files associated with this preprint. Click to download.

- GraphicalAbstract01.doc